Journal of Fluorescence (2019) 29:1089–1101
https://doi.org/10.1007/s10895-019-02420-1

ORIGINAL ARTICLE

Synthesis of Nanoparticles of ZnS:Ag-L-cysteine-protoporphyrin IX Conjugates and Investigation its Potential of Reactive Oxygen Species Production

E. Sadeghi [1,2] · Z. Mahmoodian [2] · M. Zahedifar [1,2]

Received: 11 April 2019 / Accepted: 8 July 2019 / Published online: 2 August 2019

Abstract
In this paper, L-cysteine capped Ag doped ZnS nanoparticles (NPs) were synthesized and its usage in photodynamic therapy was examined. Also, the details of the conjugation method for prepared NPs with sensitizer of protoporphyrin IX (PpIX) were reported. FT-IR studies indicate the formation of ZnS:Ag nanoparticles capped with L-cysteine and an amide-bond formation between PpIX and L-cysteine-capped ZnS:Ag NPs. The formation of ZnS:Ag NPs conjugated to protoporphyrin IX was confirmed through the use of SEM, TEM, UV-Visible, FT-IR and DLS analysis. The efficient energy transfer from ZnS:Ag to PpIX sensitizer was estimated at about 90%. The production of reactive oxygen species, including singlet oxygen and free radicals, from ZnS:Ag NPs conjugated to protoporphyrin IX, was observed using a chemical method. The production of reactive oxygen species of this conjugate indicates its potential application in photodynamic therapy.

Keywords Nanoparticles · Photodynamic therapy · ZnS:Ag · Protoporphyrin IX · Reactive oxygen species

Introduction

Today, nanotechnology and nanomaterials, have attracted considerable interest in various applied and research fields. A number of NPs can be utilized in methods which are based on the fluorescence resonance energy transfer (FRET) mechanism. These NPs have a long-term optical survival and adjustable emission properties which makes them the ideal donors in FRET studies [1–3]. The ability to create reactive oxygen species (ROS) through the donation of energy to the sensitizer (via FRET mechanism) or direct contact with oxygen molecule (energy transferring (ET) mechanism) which can be used in photodynamic therapy (PDT), is one of the most important properties of NPs [4–8]. In PDT treatment, activating a special drug with light having proper wavelength and in presence of oxygen molecules, leads to the creation of reactive oxygen species such as singlet oxygen or free radicals which can lead to the elimination of cancer cells. Among the limitations of this treatment method are the absence of penetration of visible light in tissues, and the side effects of the photosensitizers. The problem of light penetration for cancers at deeper levels can be solved using NPs afterglow. These nanoparticles have the ability to use wavelengths that the photosensitizer does not absorb and with emitting the suitable wavelength can be used as a source for activating photosensitizers [9–12]. ZnS semi-conductor quantum dots are good candidates for applications in biological systems [13–16]. This compound has the ability to be doped with rare metallic elements which can obtain remarkable optical properties and therefore has been widely used in various luminescence studies [17–19]. Doped ZnS NPs have been applied in various fields such as: imaging cancer cells [13–15], labeling cancer cells and biological sensors [15, 17, 20] and detectors [21]. Copper and cobalt co-doped ZnS NPs (ZnS:Cu,Co) coated with poly(ethylene glycol) bis(carboxymethyl) ether (PEG–COOH) have been synthesized by wet chemistry method and has been conjugated to a Photosensitizer. The ratio of ZnS:Cu,Co NPs to the TBrRh123 photosensitizer in ZnS:Cu,Co-TBrRh123 conjugates was 20 to 1. Also, the MTT assay results showed an increase in cytotoxicity in cancer cell using the ZnS:Cu,Co- TBrRh123 conjugates [22]. In

✉ E. Sadeghi
sdgh@kashanu.ac.ir

[1] Physics Department, University of Kashan, Kashan, Islamic Republic of Iran

[2] Institute of Nanoscience and Nanotechnology, University of Kashan, Kashan, Islamic Republic of Iran

another study, silver and cobalt co-doped ZnS NPs (ZnS:Ag,Co) capped with 3-mercaptopropionic acid (MPA) were produced and the emission peak at 441 nm was observed. This emission peak was nearly overlapping with PpIX absorption peak at 405 nm. Then, MPA capped ZnS:Ag,Co NPs combined with PpIX at a ratio of 20 to 1 and the results achieved through the use of this combination indicated that the cell viability in MCF-7 cells was observed to be 60% [23]. Recently, conjugates of ZnS:Mn QDs with chlorin e6 have been produced and an energy transfer from QDs to Ce6 in the conjugates has been established at about 35% [24]. However, the main purpose in systems based on luminescent nanoparticles-photosensitizer is designing and synthesizing of stable, non-toxic and water-soluble nanoparticles with the highest energy transfer efficiency to the photosensitizer [9, 10]. Since the L-cysteine is more stable, inexpensive, and non-toxic than 3-mercaptopropionic acid (MPA) as a stabilizer for the synthesis of ZnS:Ag nanoparticles [25], L-cysteine was used as a stabilizer. In this paper, the method of synthesis for ZnS:Ag NPs and their conjugation method with PpIX using the L-cysteine interface will be described. In order to obtain the highest energy transfer efficiency from nanoparticles to the photosensitizer and to increase the production of active oxygen species, the emission spectrum of nanoparticle should be perfectly matched to sensitizer absorption spectrum [9–11]. In this paper, by varying the type and amount of doping and synthesis method, we will show a different emission of doped ZnS NPs, which will match the PpIX absorption spectrum more closely in comparison with the previous studies. Also, The efficiency of ZnS:Ag NPs in production of reactive oxygen species in ZnS:Ag-L-cysteine-PpIX conjugate was demonstrated, for the first time, via an inexpensive and chemical method. In this method, for the detection of singlet oxygen and free radical, anthracenedipropionic acid (ADPA) and methylene blue (MB) were used, respectively.

Materials and Methods

Synthesis of ZnS:Ag NPs

Co- precipitation method was used to synthesis ZnS:Ag NPs according to the following reaction:

$$Zn(CH_3COO)_2 + Na_2S \rightarrow ZnS + 2Na(CH_3COO)$$

The substances used in this experiment were zinc acetate ($Zn(CH_3COO)_2$, 99.9% purity), sodium sulfide (Na_2S, 99.9% purity), Brij 35 (99.99% purity), silver nitrate ($AgNO_3$, 99.9% purity), methanol, N-hydroxy succinimide (NHS), 1-ethyl-3-(3-dimethylaminopropyl)-carbodiimide hydrochloride (EDC), deionized water, methylene blue (MB), (produced by Merck company); L-cysteine and PpIX, disodium salt of 9,10-anthracenedipropionic acid (ADPA) and dimethyl sulfoxide (DMSO) (produced by sigma-Aldrich). Initially, 0.5 g of zinc acetate was dissolved in 50 ml deionized water and was stirred for 15 min (zinc acetate solution). 0.03 g of sodium sulfide was dissolved in 20 ml deionized water (sodium sulfide solution). The solution of Brij was prepared by solving 2 g of Brij 35 in 50 ml deionized water. While the zinc acetate solution was placed on the stirrer, Brij solution was added to it. Then, silver nitrate solved in water was added to the Brij-zinc acetate solution. Finally, sodium sulfide solution was added to the previous solution. The obtained precipitate was completely separated from the solution by centrifuging. After washing the product with deionized water, it was dried in the oven for 4 h at 90°C and finally 2 h at 150 °C.

Preparation of ZnS:Ag NPs Conjugated to Protoporphyrin IX

To conjugate ZnS:Ag NPs to PpIX sensitizer, a stabilizer was used. In ZnS based materials, because of the strong effect of Zn^{+2} ions, stabilizers with (S –H) groups are often used. In this study, L-cysteine was used as the interface. To this end, NPs are initially conjugated to the interface L-cysteine and then to PpIX. The L-cysteine is then attached to ZnS NPs via the head of the sulfur (S) and stabilizes the NPs [26]. For preparing ZnS NPs-L-cysteine compound, 2 ml of L-cysteine solution was added to 5 ml of ZnS:Ag NPs solution and was stirred at 55 °C for 12 h. The final mixture was washed several times with deionized water in order to remove unbounded L-cysteine molecules. The obtained deposition was dried in an oven at 70 °C for 2 h.

Conjugating ZnS:Ag NPs Capped with L-cysteine (ZnS:Ag-L-cysteine) to PpIX

ZnS:Ag NPs and PpIX were attached using cross-linking chemistry method with modifications [27] through which water-soluble EDC and NHS are used for reacting COOH groups. COOH groups are used in cross-coupling reactions [28]. Schematic Fig. 1 shows the way by which ZnS:Ag-L-cysteine conjoins PpIX. As seen in this figure, COOH group of PpIX are activated by the use of EDC and NHS and directly combined with the amine group of ZnS:Ag-L-cysteine. By forming an amine bond between the carboxyl group of PpIX and amine group of ZnS:Ag-L-cysteine, PpIX will be conjugated to the ZnS:Ag NPs. In this regard, 1.4 mg of PpIX was dissolved in 3 ml of DMSO. 2.2 mg of EDC was subsequently added to PpIX solution and after 10 min, 1.6 mg of NHS added to it and was stirred for 15 min at room temperature. Then, 5×10^{-6} mol of ZnS:Ag-L-cysteine complex was added to the above solution and was stirred for three hours at room temperature. Finally,

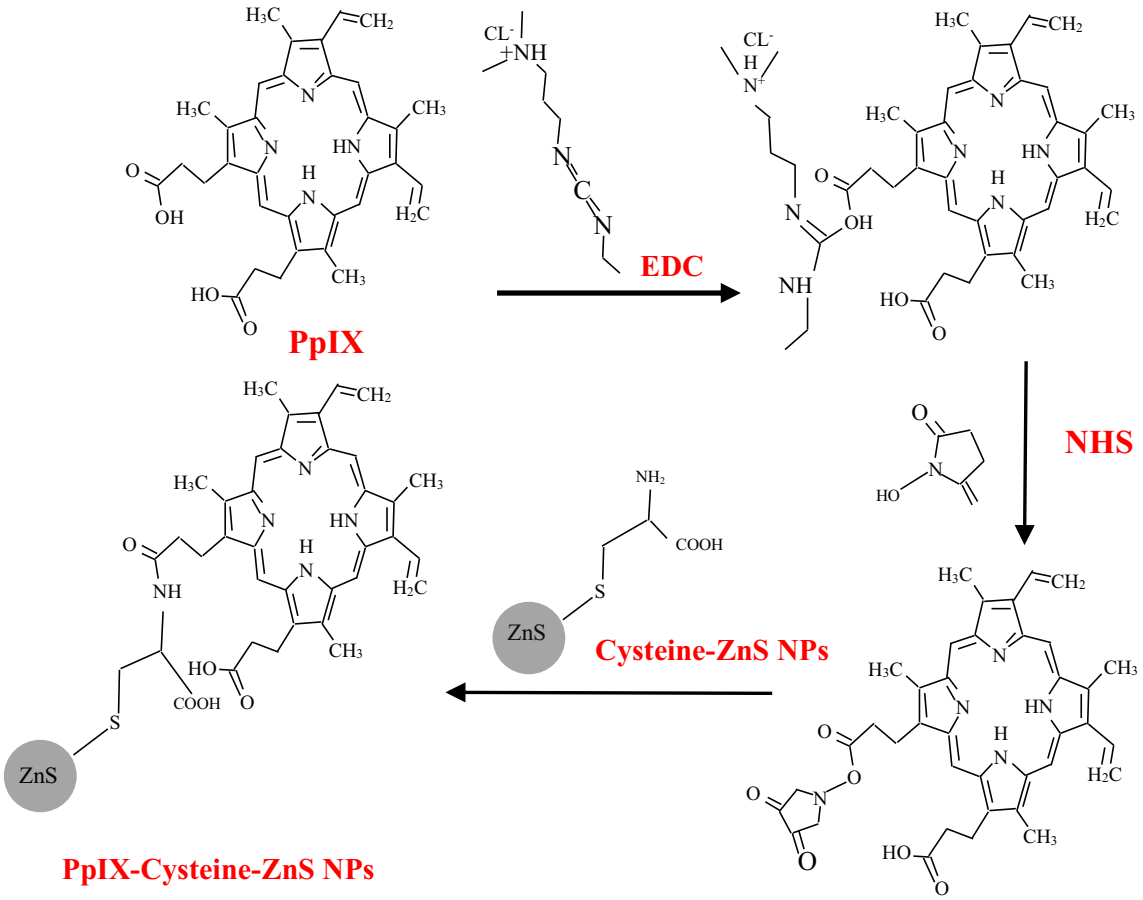

Fig. 1 The mechanism of conjugating the ZnS NPs to PpIX

ZnS:Ag NPs conjugated to the PpIX was separated by centrifuging and was washed several times with water and finally, the obtained product was dried at room temperature.

In order to study the structure of NPs and estimating the crystalline size, X-ray diffraction patterns were taken using Philips X Pert Pro MPP model, using CuK_{α} radiation, filtered by Ni. SEM images were obtained by scanning electron microscope, Hitachi S-4160. Transmission electron microscopy (TEM) of the produced samples was carried out using JEOL 2100 operating at an accelerating voltage of 200 kV. Photoluminescence spectrum was recorded by using Perkin- Elmer spectrometer, LS55 model and xenon arc. Absorption spectra were taken by Shimadzu UV-vis scanning spectrometer. ZEN3600, a dynamic light scattering device manufactured by Malvern Company, was used to obtain the particle size distribution before and after conjugation process. Magna IR 550 model was used to record the Fourier transformed infrared spectrum of the samples. UVC ultraviolet lamp, TUV 55 W HO Philips was used for exciting the NPs and investigating their capability in the production of Singlet Oxygen and free radical.

Results and Discussion

XRD

XRD diffraction pattern of ZnS:Ag NPs, as shown in Fig. 2, confirms that the structure of Zinc sulfide with a cubic crystalline structure is in correspondence to the ICSD collection code no. 067790. The spectrum peaks correspond with plates of (111), (220) and (311) which are placed at about 29, 48 and 57 angles, respectively. By substituting data, related to the main peak of plate 111, the average diameter of NPs was calculated about 24 nm using Scherrer's formula.

EDS Analysis

Figure 3, illustrates the energy dispersive spectroscopy (EDS) spectrum, which are related to the ZnS:Ag NPs. This spectrum, confirms the existence of zinc, sulfur and silver elements. The results show that the percentage of zinc and sulfur atoms are respectively 54.8% and

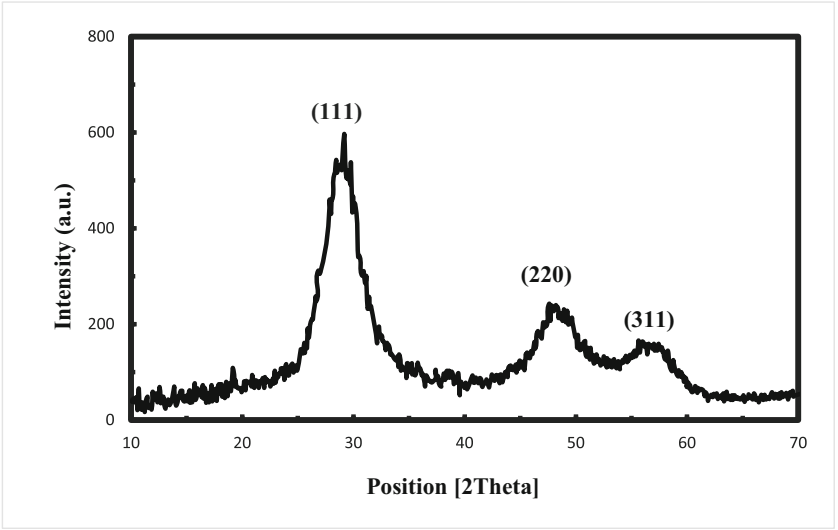

Fig. 2 X-ray diffraction pattern of synthesized ZnS:Ag NPs

44.3% and the Zn:S equal is 1:0.88. Moreover, the weight percentage of silver is about 0.9%.

FRET Mechanism

FRET is an electromagnetic phenomenon which occurs between an excited state of donor molecule (D) and an acceptor molecule (A) in the ground state. Donor molecule emits light at a wavelength that overlaps with the absorption spectrum of the acceptor [29]. By irradiating the NPs with UV light, the excited NPs transfer their energy to the PpIX acceptor and produce stimulated PpIX molecule. The stimulated PpIX molecule will attempt to stabilize by returning to the ground state. If the stimulated PpIX molecule returns directly to the ground state, it will lose its energy in the form emission of fluorescence, and if placed under intersystem crossing, it will reach an excited triplet-state. In excited triplet state of PpIX molecule, two types of reactions occur; In one type, the reaction involves the transfer of electrons or protons from PpIX molecule to nearby molecules that leads to the production of free radicals. In the second type of reaction, PpIX molecule goes from the excited triplet state to the ground state and transfers energy to the adjacent oxygen molecules, which results in the formation of singlet oxygen [10]. Figure 4 shows the energy transfer from Zns:Ag NPs to the PpIX sensitizers. The rate of energy transfer between D and A molecules depends on the degree of overlapping between D-emission spectrum, and A-absorption spectrum, the relative orientation of donor, acceptor dipole transition, and the distance between D and A molecules and quantum efficiency [29]. The absorption spectrum of PpIX sensitizer and emission spectrum of ZnS:Ag NPs can be seen in Fig. 5. According to Fig. 5, PpIX absorption spectrum contains four peaks in wavelengths of 405, 508, 542 and 580 nm. A strong emission is also observed at a wavelength of 407 nm in the emission spectrum of Zns:Ag NPs. A good overlap between the emission spectrum of synthesized NPs

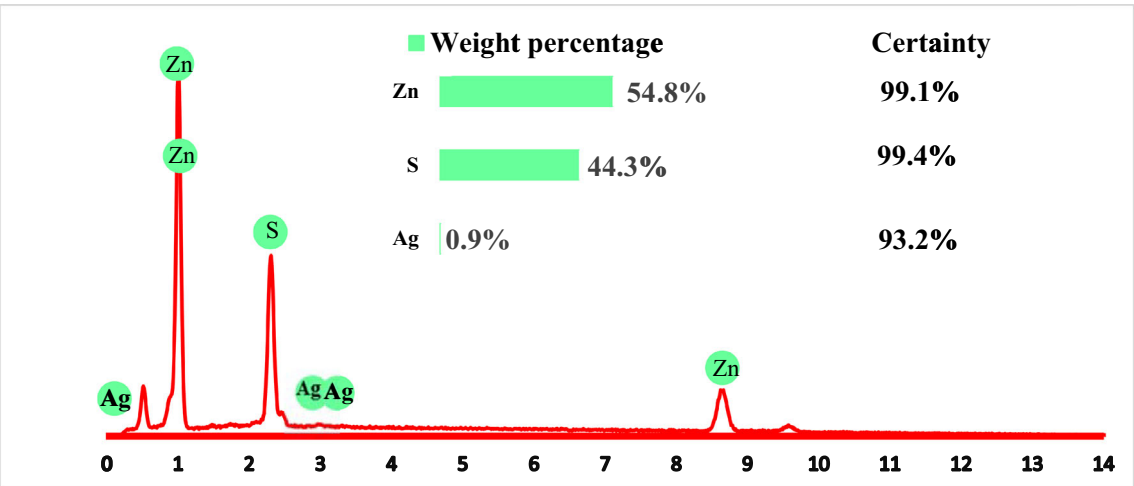

Fig. 3 EDS spectrum of ZnS:Ag NPs

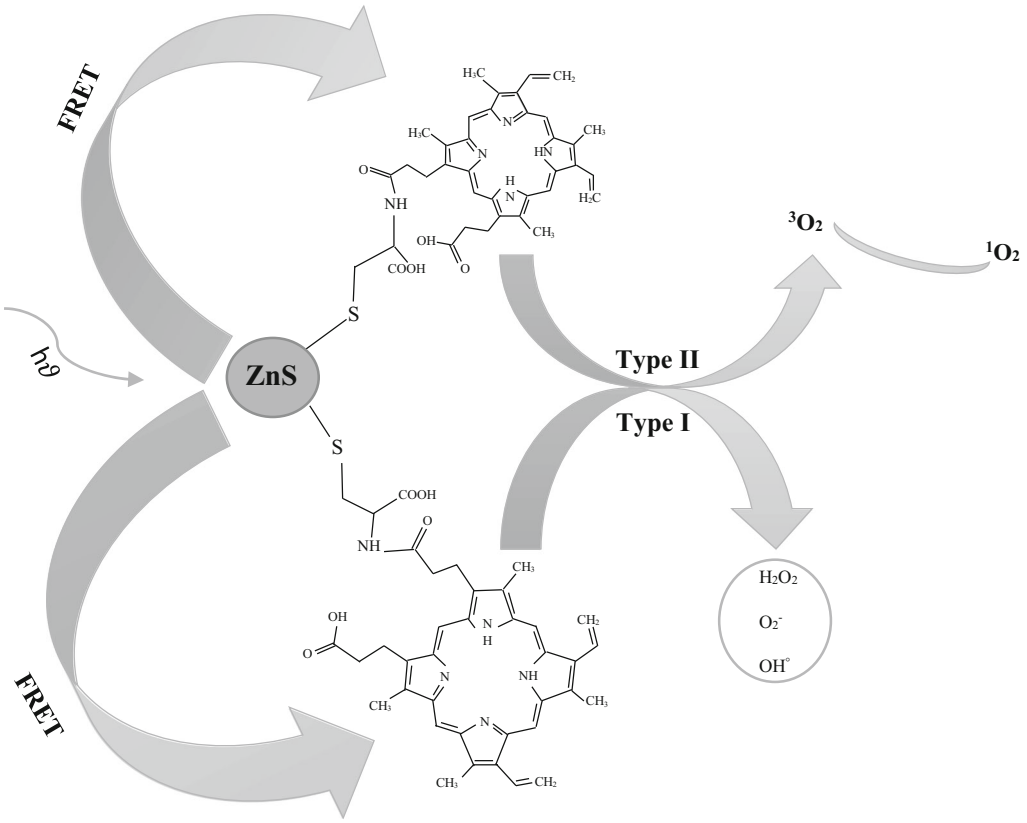

Fig. 4 A schematic of how to generate reactive oxygen species by ZnS NPs to PpIX

and the absorption spectrum of PpIX sensitizer facilitates the energy transfer from NPs to sensitizer as well as the production of singlet oxygen and free radicals.

The investigation of the energy transfer from ZnS:Ag NPs to PpIX was performed using steady-state fluorescence measurements [30, 31]. Figure 6 demonstrates the emission spectrum of ZnS:Ag NPs before and after the conjugation, under excitation at 250 nm. According to Fig. 6, the emission peaks located at 625 and 665 nm, which are related to PpIX, are observed in the emission spectrum of the ZnS:Ag

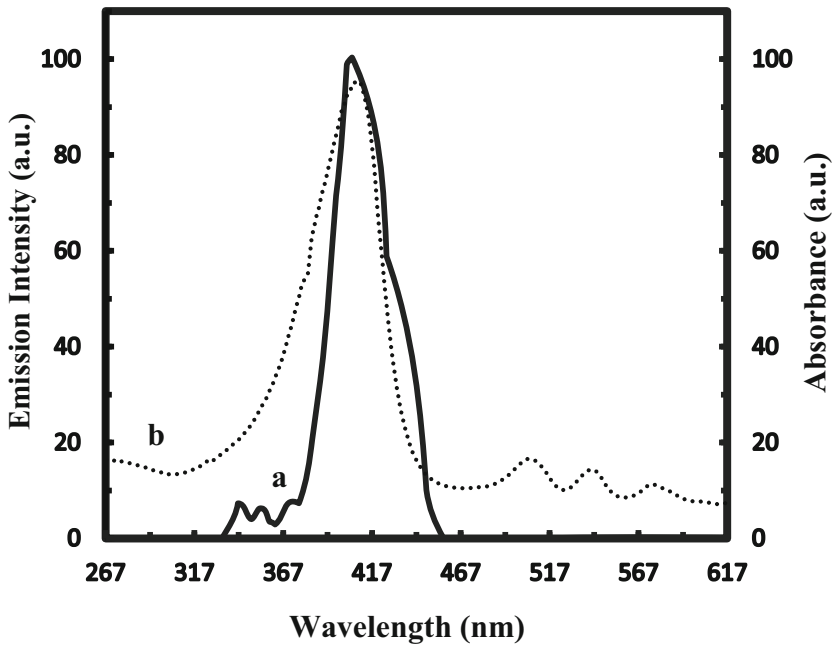

Fig. 5 Emission spectrum of ZnS:Ag NPs (**a**) and absorption spectrum of PpIX sensitizer (**b**)

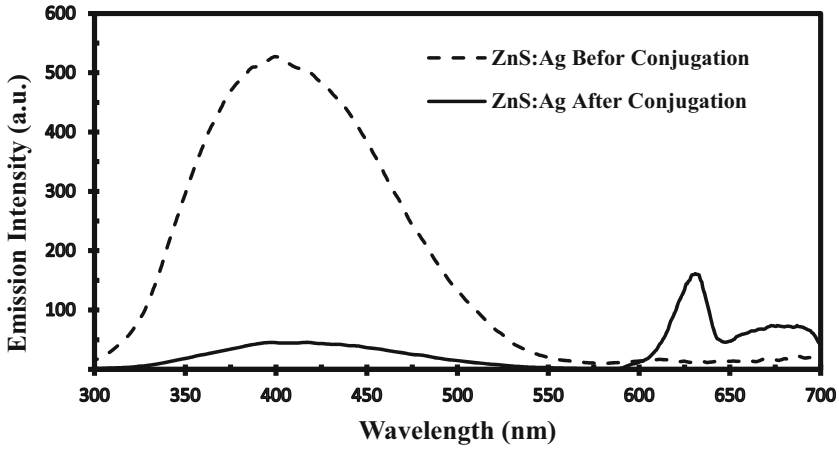

Fig. 6 Emission spectrum of ZnS:Ag NPs before and after attaching to the PpIX under excitation at 250 nm

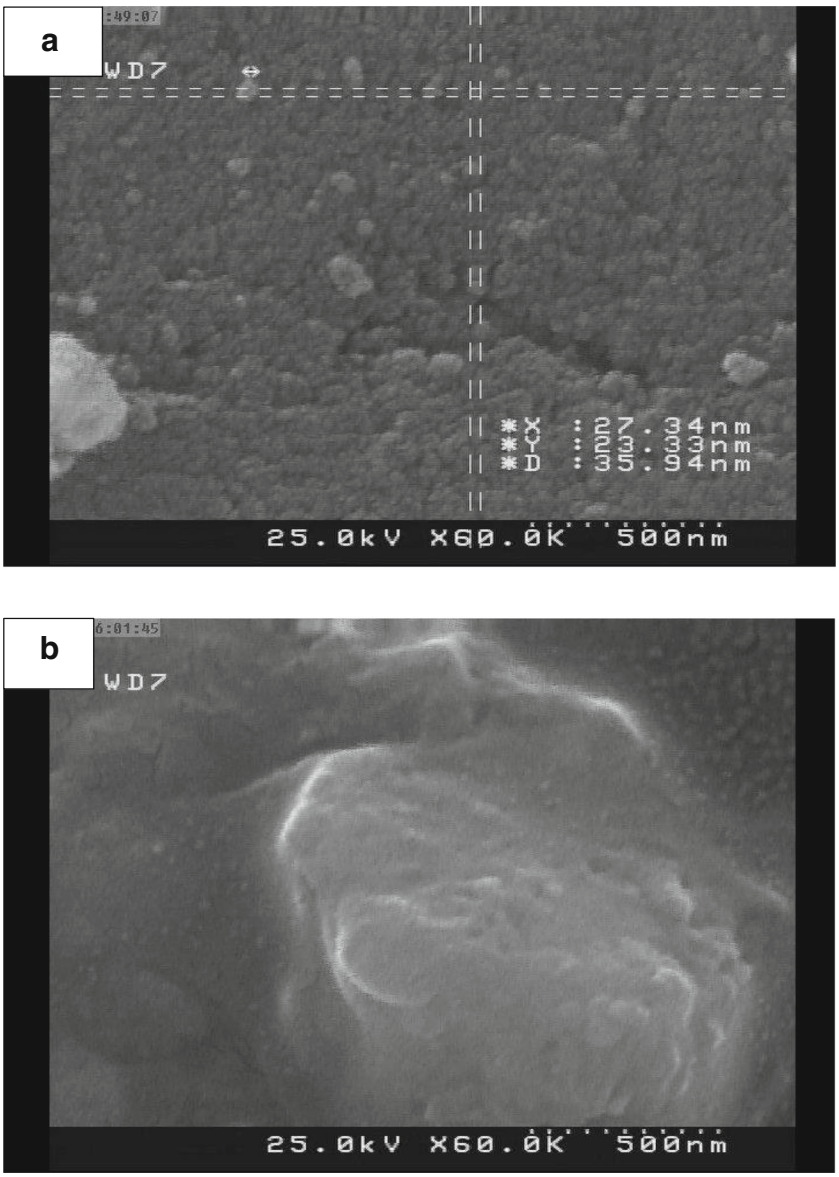

Fig. 7 SEM images of ZnS:Ag NPs (**a**) and ZnS:Ag NPs conjugated to protoporphyrin IX (**b**)

conjugated to PpIX. Also, a reduction in the emission intensity of the ZnS:Ag NPs after conjugation can be seen clearly. This phenomenon might be due to the energy transfer from the excited donor (ZnS:Ag NPs) to the acceptor (PpIX). Transmission of energy from ZnS:Ag NPs to PpIX can be a strong reason for their combination, because the effective energy transfer from the NPs to the sensitizer occurs when the NPs and the sensitizer are well attached [30–32].

The FRET efficiency can be calculated using the change of the donor emission intensity before and after attaching to the acceptor by Eq. 1 [10, 30, 32].

$$E = 1 - \frac{F_{DA}}{F_D} \quad (1)$$

where F_D and F_{DA} are, the emission intensity of ZnS:Ag NPs and ZnS:Ag NPs conjugated to PpIX (NPs-PpIX), respectively. According to the data in Fig. 6 and using Eq. 1, energy transfer efficiency is measured about 90%.

SEM, TEM and DLS Analysis

SEM images of ZnS:Ag NPs and ZnS:Ag NPs conjugated to PpIX (NPs-PpIX) were used to identify the shape and morphology of ZnS:Ag NPs. It is observed in Fig. 7 that the conjugated NPs are more fixed together in comparison with ZnS:Ag NPs which could be attributed to the conjunction of PpIX on the surface of NPs. TEM images of Fig. 8 were also taken to further clarify the above conclusion. The larger size in Fig. 8b confirms the above statement on the connection of PpIX on the surface of ZnS:Ag NPs. For a more precise observation, a DLS analysis was taken on attached and unattached samples. Figure 9 displays the NPs size distribution before and after attaching to PpIX. The maximum size is about 28 (for unattached NPs) and 58 nm (for attached NPs) which reveals how PpIX attaches to ZnS:Ag NPs as well as the growth in size.

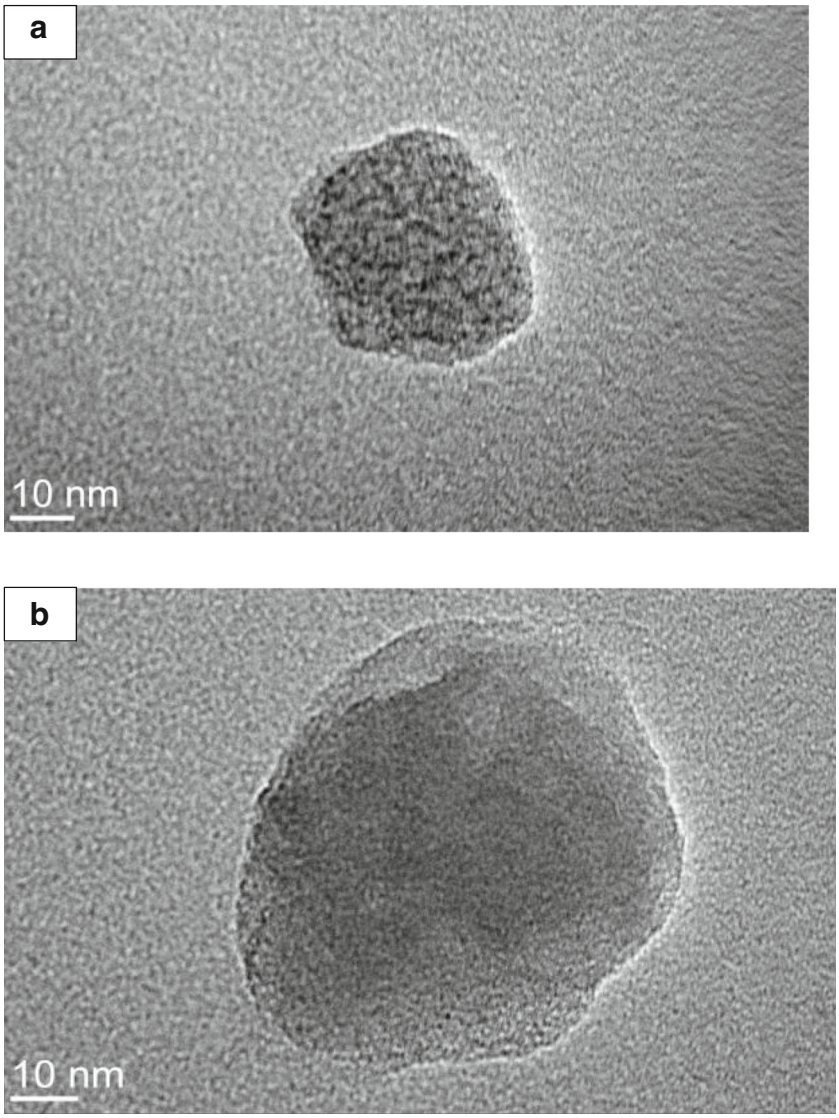

Fig. 8 TEM images of ZnS:Ag NPs (**a**) and ZnS:Ag NPs conjugated to protoporphyrin IX (**b**)

FT-IR and UV-Visible Analysis

Figure 10, shows FT-IR spectra of ZnS:Ag NPs, L-cysteine, NPs-L-cysteine and NPs-PpIX. As seen in Fig. 10a, the absorption peak in stretching vibration of 542 cm^{-1} is related to the Zn–S bond [20]. In Fig. 10b and c, associated with L-cysteine and NPs-L-cysteine, the absorption peak in the region 600–800 cm^{-1} is related to the C–S bond, and the absorption peak in district of 1550–1600 cm^{-1} is related to the carboxylic acid group (COO^{-}). Also the absorption peaks in area 2990–

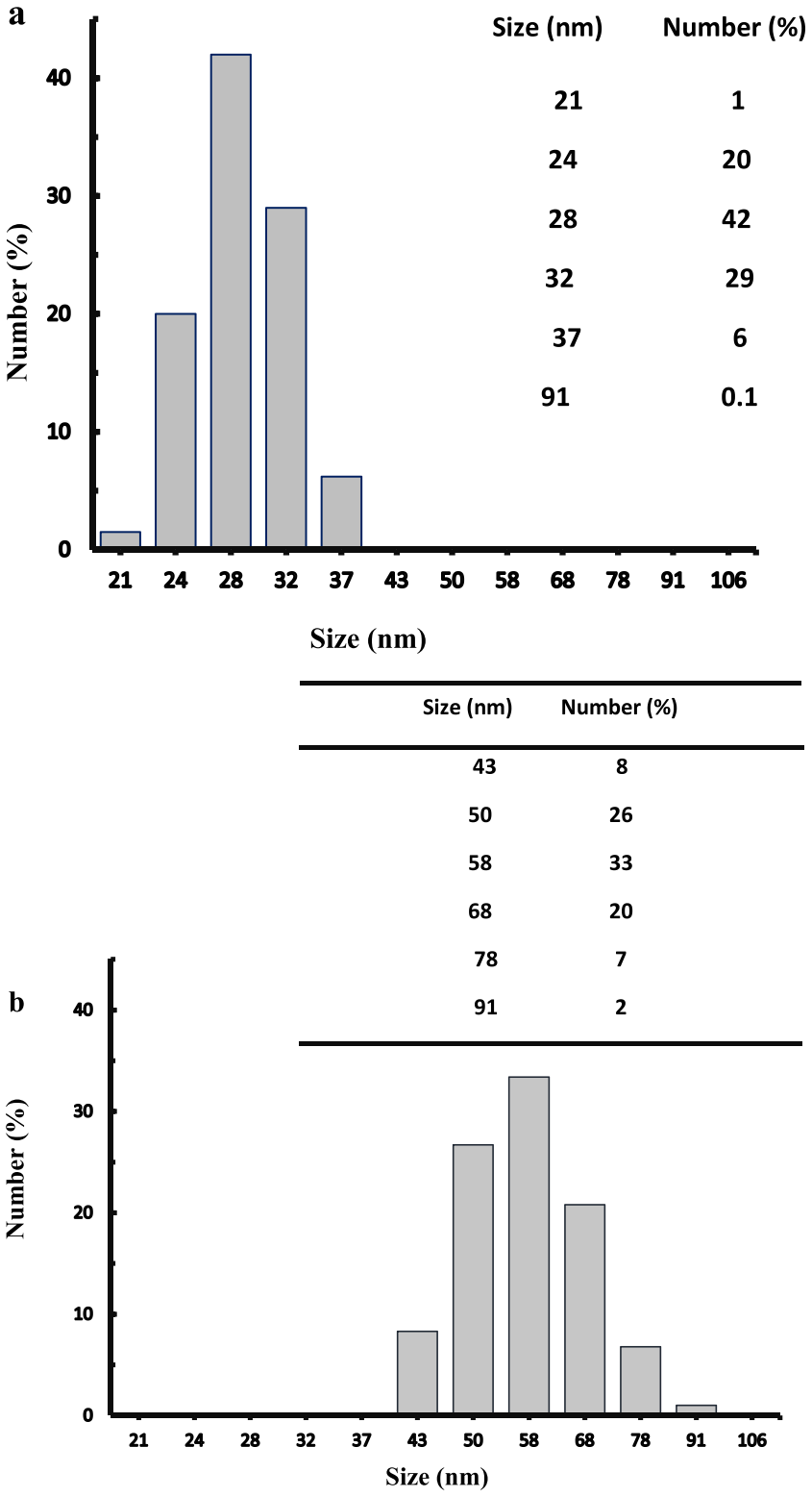

Fig. 9 The size distribution of NPs before (**a**) and after (**b**) attaching to the PpIX

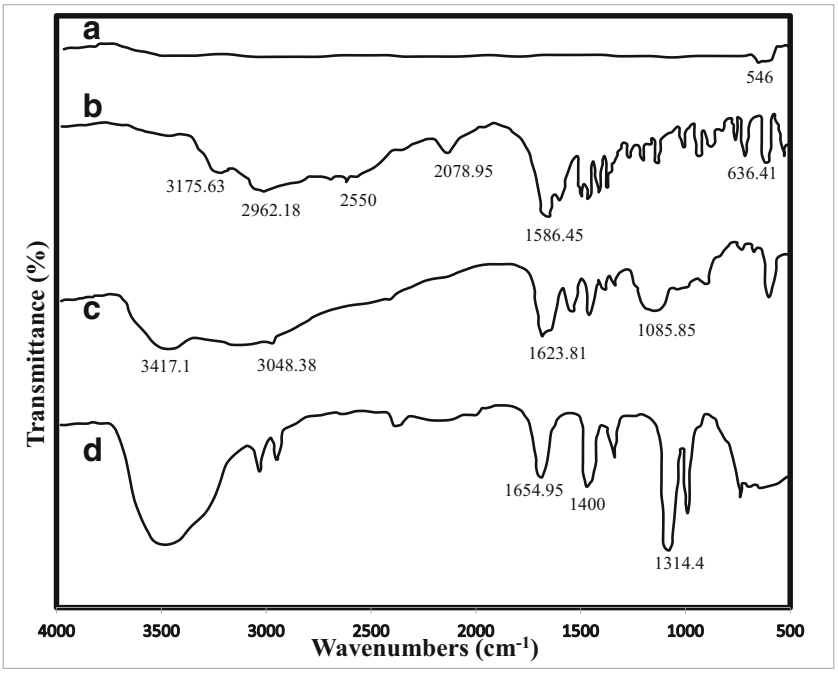

Fig. 10 FT-IR spectrum of ZnS:Ag NPs (**a**), L-cysteine (**b**), ZnS:Ag NPs capped with L-cysteine (**c**) and ZnS:Ag NPs conjugated to the PpIX (**d**)

3420 cm^{-1} shows the amino group (NH_2) which can be observed in L-cysteine and NPs-L-cysteine. However, the peak of stretching vibration related to the (S-H) bond in the district of 2550 cm^{-1}, observed in L-cysteine, is not seen in the spectrum of NPs-L-cysteine. This is due to the bond formation between ZnS:Ag NPs and thiol stabilizer group which have (S-H) bond in L-cysteine, leading to the breakdown of S-H bond and conjugation of L-cysteine to the ZnS:Ag NPs [20, 26]. Chemical conjugation between NPs-L-cysteine with PpIX occurs when COOH functional groups of PpIX react with the NH_2 functional group of L-cysteine, leading to the formation of an amide bond. Figure 10d, shows the FT-IR spectrum of NPs-PpIX. As can be seen in the spectrum of NPs-PpIX, the peak of stretching vibrations for carbonyl group (C=O) is visible in 1654.95 cm^{-1} and for C-N bond, is in 1400 cm^{-1} which indicates the formation of an amide

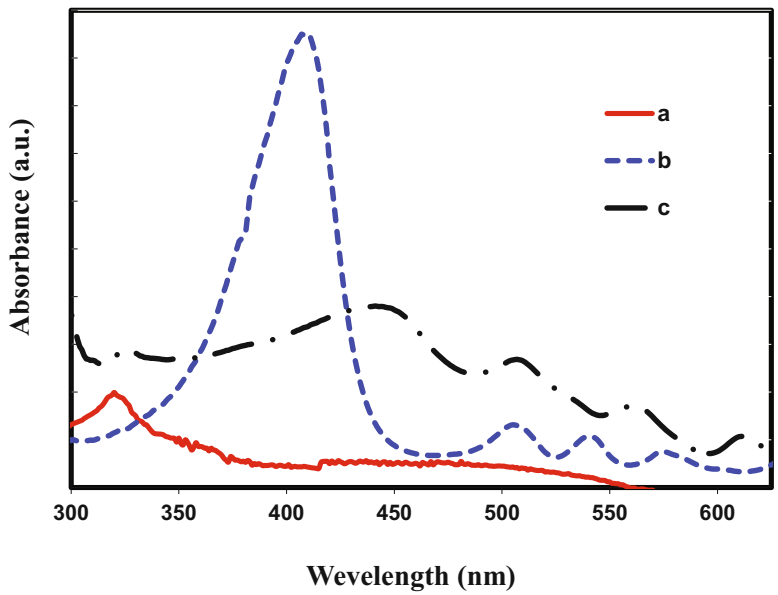

Fig. 11 The UV-visible spectrum of ZnS:Ag NPs (**a**), PpIX (**b**) and ZnS:Ag NPs conjugated to PpIX (**c**)

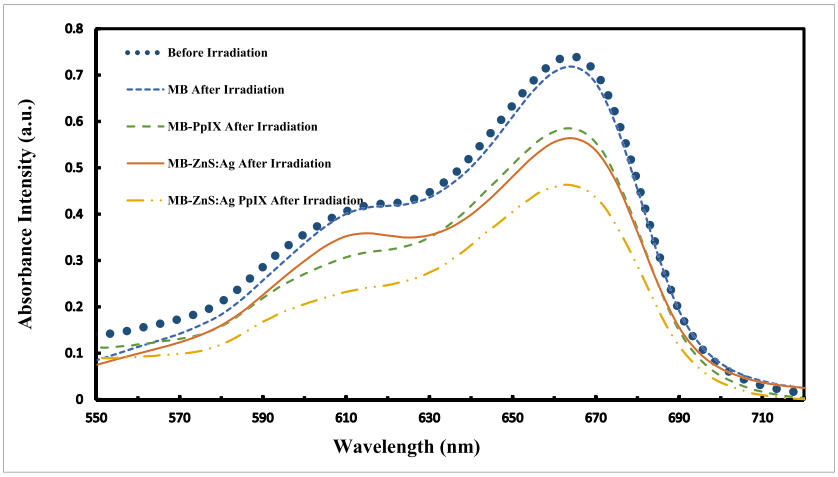

Fig. 12 Absorption spectrum of MB in four samples of MB, MB and PpIX, MB and ZnS:Ag NPs, and MB and ZnS:Ag NPs-PpIX before and after of UV irradiation

bond between NPs and PpIX [33]. The UV-visible spectrum of ZnS:Ag NPs, PpIX and NPs-PpIX, can be seen respectively in Fig.11a, b and c. In Fig. 11a, an absorption peak is seen at a wavelength of 320 nm which is shifted to the shorter wavelength (blue shifting) in comparison to the absorption peak of the bulk sample located at a wavelength of 340 nm [34]. This is a result of quantum confinement in NPs which causes the levels to shifts to higher energies. Also the wavelength corresponding to all absorption peak of NPs-PpIX (c) is shifted to a higher wavelength in comparison with that of ZnS:Ag NPs (a) (first peak of C-absorption curve is related to ZnS:Ag absorption) and PpIX (b) (Fig. 11) which can be attributed to the presence of PpIX on the surface of ZnS:Ag NPs as were previously reported for other complexes [11, 35].

Chemical Method

Detection of Free Radical

To detect free radicals generated, the methylene blue (MB) was used as a free radical sensor. The MB is a kind of dye that oxidized in the presence of free radical and decomposes into CO_2 and H_2O. According to the Beer–Lambert law, the MB concentration is associated with MB absorbance that is shown in Eq. 2 [36–38].

$$\text{Degradation efficiency} = \frac{C_0 - C}{C_0} \times 100\% = \frac{A_0 - A}{A_0} \times 100\% \quad (2)$$

In Eq. 2, C_0 and C are the concentrations of MB at t = 0 and specific time (t), respectively and A_0 and A are the MB absorbance at reaction time = 0 and reaction time = t, respectively. Therefore, the methylene blue degradation is associated with a decrease in its absorption spectrum [37, 38]. In order to investigate the production of free radicals, first, four samples, which consisted of MB, MB–PpIX, MB-ZnS:Ag, MB-ZnS:Ag-PpIX, were made with the same concentrations. First, the absorption spectra of all of these samples were recorded by a spectrophotometer. Then, the samples were exposed to UV irradiation for 20 min. After the irradiation, their absorption spectrum was again recorded in the same conditions as before. As explained, investigating the production of free radical

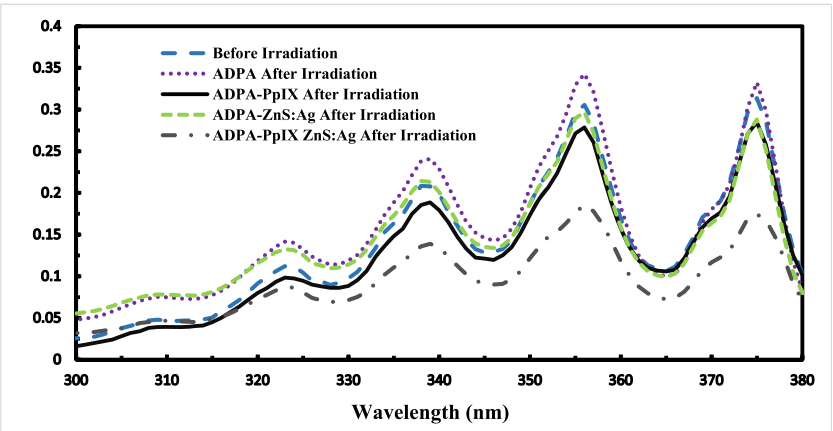

Fig. 13 Absorption spectrum of ADPA in four groups of ADPA, ADPA and PpIX, ADPA and ZnS:Ag NPs, and ADPA and ZnS:Ag NPs-PpIX before and after of UV irradiation

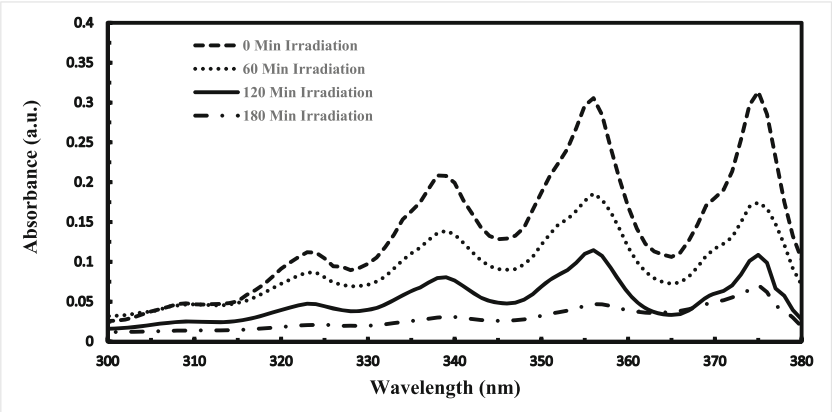

Fig. 14 Absorption spectrum of ADPA in ADPA and ZnS:Ag NPs-PpIX group before and after 1, 2 and 3 h UV irradiation

from the change in absorption intensity of MB before and after irradiation was performed. In Fig. 12. the absorption spectra of MB before and after the UV irradiation are shown in these samples. As seen from this figure, a more severe reduction in the absorption intensity of the MB has occurred in MB-PpIX-ZnS:Ag sample after the UV irradiation. This absorption intensity reduction can be due to free radical production based on the type I reaction.

Detection of Singlet Oxygen

For investigating the role of ZnS:Ag NPs conjugated to PpIX, to produce singlet oxygen, the disodium salt of 9,10-anthracenedipropionic acid (ADPA) was used as a singlet oxygen sensor. When ADPA is placed adjacent to the singlet oxygen, it reacts with singlet oxygen to be converted its endoperoxide form. The emission and absorption spectra of endoperoxide is not within range of emission and absorption spectra of APDA. So, the reduction of emission and absorption intensity of ADPA, results in the production of singlet oxygen [39–41]. As explained earlier, the PpIX sensitizer has a strong absorption at 405 nm which fairly overlaps with emission bond of the ZnS:Ag NPs (wavelength of 407 nm). Therefore, ZnS:Ag NPs are a good candidate for activation of PpIX sensitizer. For the evaluation of this ability, four groups of ADPA, ADPA-PpIX, ADPA-ZnS:Ag NPs, and ADPA-ZnS:Ag NPs-PpIX were prepared. The absorption spectra of these four groups, an hour before and after UVC light irradiation were recorded. The results are presented in Fig. 13. According to this figure, the absorption intensity of ADPA-NPs-PpIX group has significantly reduced after UV irradiation, while the other three groups did not show such a decrease. The reason for the decrease in the absorption intensity of ADPA of this group, compared with other groups, is the singlet oxygen production based on type II reaction. To optimize the irradiation time, ADPA -NPs-PpIX group was irradiated to UV light at different time intervals. The results were plotted in Fig. 14. The reduction of absorption intensity of ADPA - NPs-PpIX group was examined by increasing the irradiation time from 1 h to 3 h. By irradiating the sample for 3 h, the absorption intensity reduces by 7 times compared to the absorption intensity before the irradiation. It means that by increasing the duration of the irradiation, the

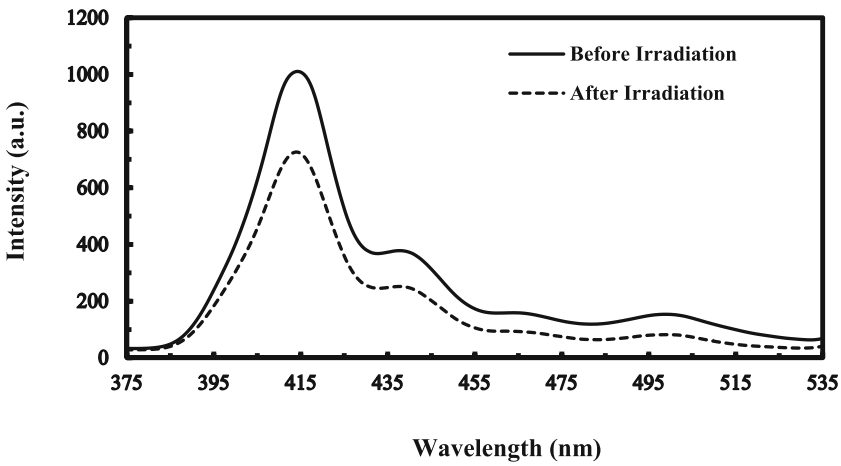

Fig. 15 PL emission of ADPA in ADPA and ZnS:Ag NPs-PpIX group before and after 30 min UV irradiation

number of produced singlet oxygen increases. Due to the effect of singlet oxygen toxicity, an increase in its production can lead to increased toxicity of the solution and justifies the capability of the produced sample to destroy the cancer cells and be used in photodynamic therapy.

Finally, the efficiency of ZnS:Ag NPs - PpIX in the production of singlet oxygen, was more elucidated using the emission spectrum of ADPA and comparing its intensity, before and after the UV irradiation. The emission spectrum of ADPA soluble was obtained by fluorescence spectrometer 30 min before and after the irradiation and its emission spectrum was recorded. As seen in Fig. 15, ADPA emission intensity decreased significantly after the irradiation which in turn confirms the production of singlet oxygen in presence of NPs through FRET mechanism. Given the relatively long lifespan of the synthesized NPs, it is possible that the conjugated NPs illuminated by UV light outside the body, and then be carried toward the deep tumors in the tissue. By doing so, the problem of using UV radiation (low penetration through the biological layer and potentially harmful to tissue) to stimulate the sample can be solved.

Conclusion

Using FRET mechanism and production of reactive oxygen species, this study investigated the ability of ZnS:Ag NPs, as an energy donor to the photosensitizing agent of PpIX as an energy acceptor. We evaluated the production of reactive oxygen species (singlet oxygen and free radical) by ZnS:Ag NPs, PpIX and ZnS:Ag-PpIX conjugation using an optical method. The emission peak of the prepared NPs was located at 407 nm that is matched with PpIX absorption peak in 405 nm. In order to synthesize stable and non-toxic conjugation, ZnS:Ag NPs were coated with L-cysteine successfully. Then, L-cysteine capped ZnS:Ag NPs were conjugated to the PpIX as a sensitizer and the stable ZnS:Ag-L-cysteine-PpIX nanosystem was created. Due to the use of L-cysteine as an interface for binding NPs ZnS:Ag and PpIX, the nanoparticles were attached to the sensitizer in a ratio of about 2 to 1. The results of energy transfer studies shows that the conjugating of ZnS:Ag NPs and PpIX has been successfully done. The results also showed that more reactive oxygen species can be produced by ZnS:Ag NPs conjugated to PpIX. The production of singlet oxygen grows by increasing the duration of UV irradiation. The use of nanoparticles conjugated to PpIX significantly increases the production of reactive oxygen species compared to PpIX alone. This means that ZnS:Ag NPs have the capability to be used as an energy donor in photodynamic therapy.

Acknowledgements The authors gratefully acknowledge the research council of the University of Kashan for financial support of this work.

References

1. Willard DM, Carillo LL, Jung J, Orden AV (2001) CdSe–ZnS quantum dots as resonance energy transfer donors in a model protein–protein binding assay. Nano Lett 1:469–474
2. Mamedova NN, Kotov NA, Rogach AL, Studer J (2001) Albumin −CdTe nanoparticle bioconjugates: preparation, structure, and interunit energy transfer with antenna effect. Nano Lett 1:281–286
3. Bankole OM, Achadu OJ, Nyokong T (2017) Nonlinear interactions of zinc Phthalocyanine-graphene quantum dots nanocomposites: investigation of effects of surface functionalization with heteroatoms. J Fluoresc 27:755–766
4. Samia CS, Chen X, Burda C (2003) Semiconductor quantum dots for photodynamic therapy. J Am Chem Soc 125:15736–15737
5. Managa M, Ngoy BP, Nyokong T (2019) Photophysical properties and photodynamic therapy activity of a meso-tetra(4-carboxyphenyl)porphyrin tetramethyl ester–graphene quantum dot conjugate. New J Chem 43:4518–4524
6. Matshitse R, Nyokong T (2018) Singlet oxygen generating properties of different sizes of charged graphene quantum dot Nanoconjugates with a positively charged Phthalocyanine. J Fluoresc 28:827–838
7. Idowu M, Chen JY, Nyokong T (2008) Photoinduced energy transfer between water-soluble CdTe quantum dots and aluminium tetrasulfonated phthalocyanine. New J Chem 32:290–296
8. Tshangana C, Nyokong T (2015) The Photophysical properties of multi-functional quantum dots-magnetic nanoparticles-indium Octacarboxyphthalocyanine nanocomposite. J Fluoresc 25:199–210
9. Chen W (2008) Nanoparticle self-lighting photodynamic therapy for cancer treatment. J Biomed Nanotechnol 4:369–376
10. Chen W (2008) Nanoparticle fluorescence based technology for biological applications. J Nanosci Nanotechnol 8:1019–1051
11. Zahedifar M, Sadeghi E, Shanei MM, Sazgarnia A, Mehrabi M (2016) Afterglow properties of CaF_2:Tm nanoparticles and its potential application in photodynamic therapy. J Lumin 171:254–258
12. Tavakkli F, Zahedifar M, Sadeghi E (2018) Effect of LaF_3:Ag fluorescent nanoparticles on photodynamic efficiency and cytotoxicity of Protoporphyrin IX photosensitizer. Photodiagn Photodyn Ther 21:306–311
13. Manzoor K, Johny S, Thomas D, Setua S, Menon D, Nair S (2009) Bio-conjugated luminescent quantum dots of doped ZnS: a cyto-friendly system for targeted cancer imaging. Nanotechnology 20:065102
14. Chen L, Liu Y, Lai C, Berry RM, Tam KC (2015) Aqueous synthesis and biostabilization of CdS@ZnS quantum dots for bioimaging applications. Mater Res Express 2:105401
15. Mathew ME, Mohan JC, Manzoor K, Nair SV, Tamura H, Jayakumar R (2010) Folate conjugated carboxymethyl chitosan-manganese doped zinc sulphide nanoparticles for targeted drug delivery and imaging of cancer cells. Carbohydr Polym 80:442–448
16. Masteri-Farahani M, Mahdavi S, Khanmohammadi H (2018) Chemically functionalized ZnS quantum dots as new optical nanosensor of herbicides. Mater Res Express 5:035055
17. Murase N, Jagannathan R, Kanematsu Y, Watanabe M, Kurita A, Hirata K, Yazawa T, Kushida T (1999) Fluorescence and EPR characteristics of Mn^{2+} −doped ZnS nanocrystals prepared by aqueous colloidal method. J Phys Chem B 103:754–760
18. Yang P, Lu M, Xu D, Yuan D, Zhou G (2001) Photoluminescence properties of ZnS nanoparticles co-dope with Pb^{2+} and Cu^{2+}. Chem Phys Lett 336:76–80
19. Kim JY, Park SH, Jeong T, Bae MJ, Kim YC, Han I, Yu S (2010) High electroluminescence of the ZnS:Mn nanoparticle/cyanoethylresin polymer/single-walled carbon nanotube composite using the tandem structure. J Mater Chem 22:20158–20162

20. Aswathy J, Jahnavi S, Krishna R, Manzoor K, Nair S, Menon D (2011) Targeted labeling of cancer cells using biotin tagged avidin functionalized biocompatible fluorescent nanocrystals. J Nanosci Nanotechnol 11:7611–7620
21. Wang CL, Gou L, Zaleski JM, Friesel DL (2010) ZnS quantum dot based nanocomposite scintillators for thermal neutron detection. Nucl Instrum Methods A 622:186–190
22. Ma L, Zou X, Bui B, Chen W, Song KH, Solberg T (2014) X-ray excited ZnS:Cu,Co afterglow nanoparticles for photodynamic activation. Appl Phys Lett 105:013702
23. Ma L, Zou X, Hossu M, Chen W (2016) Synthesis of ZnS:Ag,Co water-soluble blue afterglow nanoparticles and application in photodynamic activation. Nanotechnology. 27:315602
24. Visheratina AK, Loudon A, Kuznetsova VA, Orlova AO, Gun'ko YK, Baranov AV, Fedorov AV (2018) Water-soluble conjugates of ZnS:Mn quantum dots with chlorin e6 for photodynamic therapy. Opt Spectrosc 125:94–98
25. Huang F, Lan Y, Lan P (2011) Synthesis and characterization of water-soluble L-cysteine-modified ZnS nanocrystals doped with silver. J Mater Sci 46:5732–5736
26. Kumar S, Singhal M, Sharma JK (2013) Functionalization and characterization of ZnS quantum dots using biocompatible L-cysteine. J Mater Sci Mater Electron 24:3875–3880
27. Grabarek Z, Gergely J (1990) Zero-length crosslinking procedure with the use of active esters. Anal Biochem 185:131–135
28. Bartczak D, Kanaras AG (2011) Preparation of peptide functionalized gold nanoparticles using one pot EDC/sulfo-NHS coupling. Langmuir. 27:10119–10123
29. Clegg RM (1995) Fluorescence resonance energy transfer. Curr Opin Biotechnol 6:103–110
30. Yaghini E, Seifalian AM, MacRobert AJ (2009) Quantum dots and their potential biomedical applications in photosensitization for photodynamic therapy. Nanomedicine 4: 353–363
31. Yaghini E, Giuntini F, Eggleston IM, Suhling K, Seifalian AM, MacRobert AJ (2014) Fluorescence lifetime imaging and FRET-induced intracellular redistribution of Tat-conjugated quantum dot nanoparticles through interaction with a phthalocyanine photosensitizer. Small 10:782–792
32. Liu Y, Zhang Y, Wang S, Pope C, Chen W (2008) Optical behaviors of ZnO-porphyrin conjugates and their potential applications for cancer treatment. Appl Phys Lett 92:143901
33. Barth A, Zscherp C (2002) What vibrations tell us about proteins. Q Rev Biophys 35:369–430
34. Corrado C, Jiang Y, Oba F, Kozina M, Bridges F, Zhang JZ (2009) Synthesis, structural, and optical properties of stable zns:cu,cl nanocrystals†. J Phys Chem A 113:3830–3839
35. Vanitha Kumari G, JothiRajanm MA, Mathavan T (2018) Pectin functionalized gold nanoparticles towards singlet oxygen generation. Mater Res Express 5:085027
36. Wang K, Yu L, Yin S, Li H, Li H (2009) Photocatalytic degradation of methylene blue on magnetically separable FePc/Fe3O4 nanocomposite under visible irradiation. Pure Appl Chem 81:2327–2335
37. Abdollahi Y, Abdullah AH, Zainal Z, Yusof NA (2011) Photocatalytic degradation of p-cresol by zinc oxide under UV irradiation. Int J Mol Sci 13:302–315
38. Mansur AAP, Mansur HS, De Souza PP, Ramanery FP, Carlos L, Souza PP (2014) ' Green ' colloidal ZnS quantum dots / chitosan nanophotocatalysts for advanced oxidation processes : study of the photodegradation of organic dye pollutants. Appl Catal B Environ. 158:269–279
39. Craig RA, McCoy CP, Baróid ATD, Andrews GP, Gorman SP, Jones DS (2015) Quantification of singlet oxygen generation from photodynamic hydrogels. React Funct Polym 87:1–6
40. Qi ZD, Li DW, Jiang P, Jiang FL, Li YS, Liu Y, Wong WK, Cheah KW (2011) Biocompatible CdSe quantum dot-based photosensitizer under two-photon excitation for photodynamic therapy. J Mater Chem 21:2455–2458
41. Liu Y, Chen W, Wang S, Joly AG (2008) Investigation of water-soluble x-ray luminescence nanoparticles for photodynamic activation. Appl Phys Lett 92:043901